Astron. Astrophys. 332, 825–841 (1998)

ASTRONOMY AND ASTROPHYSICS

An X-ray study of the PMS population of the Upper Sco-Cen association

S. Sciortino[1], **F. Damiani**[1], **F. Favata**[2], **and G. Micela**[1]

[1] Istituto e Osservatorio Astronomico G.S. Vaiana, Piazza del Parlamento 1, I-90138 Palermo, Italy (sciorti@oapa.astropa.unipa.it, damiani@oapa.astropa.unipa.it, gmicela@oapa.astropa.unipa.it)

[2] Astrophysics Division - ESA/ESTEC, Postbus 299, 2200 AG Noordwijk, The Netherlands (fabio.favata@astro.estec.esa.nl)

Received 3 July 1997 / Accepted 27 October 1997

Abstract. We have searched for low-mass pre-main-sequence stars in the nearby Upper Sco-Cen star-forming region using ROSAT observations analyzed with an innovative source detection method based on wavelet transforms. In a 5.2 ksec ROSAT PSPC image we find 32 sources down to a limiting flux of 3.9 10^{-14} erg cm^{-2} s^{-1}. In two HRI observations that cover with greater sensitivity approximately one-third of the same region we find 17 sources, down to a limiting flux of 1.4 10^{-14} erg cm^{-2} s^{-1}. Half of the HRI sources were not detected either in the PSPC pointed observation nor are they reported in the ROSAT Bright Source Catalog, nor in the final analysis of Einstein IPC data of the same region, which resulted in the detection of 18 sources down to a limiting flux of 9.1 10^{-14} erg cm^{-2} s^{-1}. Considering all the available X-ray data together, we have a total of 50 distinct X-ray sources, of which only 13 were previously reported as Einstein IPC sources in a sky region of nearly the same area as that surveyed in the present work. Our new analysis allows us to largely increase the census of likely PMS stars in the Upper Sco-Cen region and shows that the IPC survey of PMS stars in this region by Walter and collaborators is more severely incomplete than previously reported. The likely PMS nature of the stellar counterparts of the faint X-ray sources is supported by follow-up optical spectroscopy of some of these sources, as well as by the presence of variability of X-ray emission in a substantial fraction of them, and by the characteristics of available X-ray spectral information.

Key words: stars: coronae – stars: pre-main sequence – stars: late-type – stars: variables: other – X-rays: stars – open clusters and associations: individual: Upper Sco-Cen

1. Introduction

Pre-main sequence stars which have already shed their accretion disk are very hard to identify optically, as their only distinctive signs are weak Balmer emission and strong lithium absorption. They are therefore known as Weak-lined T-Tauri Stars (WTTS). Yet their identification is fundamental to study the young low mass star population, as they appear to outnumber Classical T-Tauri Stars (CTTS) in star forming regions (SFR's). X-ray observations of star-forming regions (SFR) are the best way of identifying WTTS's, as those stars are very active, with X-ray luminosities a factor 100 or more higher than corresponding normal main sequence objects of the same spectral type. The Upper Scorpius association, also know as Sco OB2-2 or Upper Sco-Cen Association (USCA), is the youngest part of the Sco-Cen-Lupus star forming region (de Geus et al., 1989; Blaauw, 1991). It has a distance module of about 6 mag (de Geus, 1992) corresponding to a distance of 160 pc, and an age, derived from the position of B stars in the H-R diagram, of 5–6 10^6 years. The USCA lies within an expanding HI shell and seems to be different from many other SFR's region surveyed in X-rays, including the near ρ Oph complex, since there is no evidence of ongoing star formation and only a small amount of dark clouds and molecular gas, since material has been swept out in the last 1–2 Myr by a supernova explosion and by strong stellar winds (de Geus, 1992). The USCA is a very good place to investigate if and how the star forming process in OB association is different from those at work in T-Tauri association and, in particular, to compare the spread of stellar ages between these two classes of SFR regions.

Before the *Einstein* IPC X-ray survey of the USCA (Walter et al., 1994, hereafter WVMBM), only 4 CTTS stars were know in the region (Herbig & Robbin-Bell, 1988). WVMBM have performed an X-ray survey (over an area of $\sim$ 7 square degree) of the USCA reporting that 24 out of 48 sources have as counterpart a PMS star. They have studied for the first time the low mass star population in this nearby SFR. This survey has allowed WVMBM to constrain the initial mass function (IMF) down to ~ 0.3 M$_\odot$ for such a young population. However this work suffers of an unavoidable bias, which unfortunately affects their conclusions: in fact, the limiting X-ray sensitivity of the WVMBM survey was such that only sources with $L_X \geq 3\ 10^{29}$erg s^{-1} could be detected. WVMBM made the assumption "that the luminosity function of the complete

Send offprint requests to: S. Sciortino

Table 1. Characteristics of the observations

Instrument	Identificator	RA [J2000]	DEC [J2000]	Exp. Time [Ksec]	Obs. Start	Obs. Span [days]
Einstein IPC	I5936	15 55 30.7	-23 43 43.5	9.72	11/2/80	1
Einstein IPC	I5997	16 00 19.6	-22 36 55.4	2.76	16/2/80	1
ROSAT PSPC	RP201024n00	15 55 00.0	-23 47 24.0	3.35	25/02/93	2
ROSAT PSPC	RP201024a01	”” ”” ””	”” ”” ””	1.85	09/08/93	10
ROSAT HRI	RH202053n00	15 56 26.0	-23 37 48.0	30.1	06/09/95	4
ROSAT HRI	RH202042n00	15 57 48.0	-23 05 24.0	3.67	28/02/95	1

sample is the luminosity function of those stars detected in the deepest exposures”; this, taken together with the shallow limiting X-ray luminosity is likely to bias their conclusions on the shape and normalization of the IMF, as well as on the history of star formation and (possible) presence of an older low-mass star population. In fact, they did not detect *any* star with mass smaller than $\sim 0.3\,M_{\odot}$, which, given the observed correlation between mass and X-ray luminosity of the most X-ray active PMS stars (Feigelson et al., 1993), could entirely be due to the shallow X-ray limiting sensitivity. Indeed they state that the mean completeness level of their sample is $\sim 33\%$, with a pronounced mass dependence of the incompleteness that is even larger below $\sim 0.5\,M_{\odot}$.

In order to verify the effect introduced by the shallow limiting X-ray sensitivity (as well as by the limited IPC angular resolution) we have carried on a deeper X-ray survey on an area of $\sim$ 3 square degrees in the USCA. In particular, we have carried on a deep pencil-beam survey of a small region ($\sim$ 40 arcmin diameter), contained within the area surveyed by WVMBM (in fact within the area in which WVMBM's survey is deepest), using the ROSAT HRI, and reaching a limiting sensitivity one order of magnitude deeper than WVMBM, i.e. down to $L_{\rm X} \sim 5\ 10^{28}$ erg s^{-1} for sources at the distance of Upper Sco-Cen. The area surveyed contains 3 of WVMBM's sources, yet we find 10 additional sources at fainter X-ray luminosities.

The present paper is organized as follows: in Sect. 2 we present the X-ray data and their analysis, in Sect. 3 we present the Log N – Log S for the X-ray sources in the region we have surveyed, in Sect. 4 we discuss the short- and long-term variability of the X-ray emission of detected sources, in Sect. 5 we report the catalog identification of the X-ray sources, in Sect. 6 the follow-up optical identifications for a few of the detected sources, finally in Sect. 7 we discuss and summarize our findings. We report in the Appendix the finding charts for the X-ray sources in our final list having an error circle of size small enough to make the identification process feasible.

2. X-Ray observations and analysis

The Upper Sco-Cen region has been observed with the ROSAT Position Sensitive Proportional Counter (PSPC; Pfefferman et al., 1986) for a total of 5200 sec (PI: F. Walter) in two distinct segments (cf. Table 1). The PSPC $\sim 1^{\circ}$ radius field of view was centered on the B2 star HD 142184. The Upper Sco-Cen association members in this image fall at off-axis angles ranging between 10 and 50 arcmin, namely in a region where the FWHM of the PSPC point spread function (PSF) varies from 18 to 130 arcsec.

The *Einstein* IPC source list published by WVMBM includes 13 sources in the two IPC fields we have considered. The characteristics of these images are summarized in Table 1 together with those of the other observations we have analyzed. The final processing and archiving of Einstein IPC stellar data (Harnden et al., 1990; Sciortino et al., 1988) shows the existence of 5 further weaker sources[1] making the Upper Sco-Cen region a place with a quite high concentration of X-ray emitters, likely associated with PMS stars (cf. Sect. 6). The list of all the Einstein IPC sources found by the final data processing is given in Table 2, where the flag in the last column indicates if a source was previously reported by WVMBM. The chosen source acceptance criterion is such that no more than one spurious detection is expected among the list of 18 IPC detections (Harnden et al., 1984). For easy comparison with the new ROSAT data, the X-ray flux has been computed in the (0.2 – 2.0 keV) bandpass. Given the lack of data in individual source absorption and temperature for most of the sources the conversion factor from count-rate to flux has been evaluated for Log N_H in the 20.65–21.20 range (corresponding to the range of A_V 0.1–0.8 measured by WVMBM for stars in that regions as well as to the range of N_H deduced from the spectral fits discussed in Sect. 4.4) and for an optically thin emitting plasma with a single temperature in the 0.5–1.4 keV range. The adopted conversion factors are 2.92 10^{-11} and 3.78 10^{-11} erg cm^{-2} cnt^{-1} for the rates in the IPC (0.16–3.5 keV) and (0.8–3.5 keV) energy bands, respectively. The uncertainties in derived X-ray fluxes, due to the range of admissible temperature and absorption is $\leq 50\%$, dominating the uncertainty in derived flux even for the weakest source.

To overcome the problem posed by the limited sensitivity and angular resolution of the *Einstein* and of the PSPC observations we have obtained a deep (30 ksec) HRI observation (WG202053H, PI: F. Favata) that was conceived as a follow-up study of the Einstein observation Seq. 5997 and that, post-facto, has resulted in an (unplanned) follow-up of the archive PSPC observation we have analyzed. In order to increase the limiting sensitivity in the external region of the PSPC image and of the IPC image 5936, we have retrieved from the ROSAT archive

[1] These sources are not listed in the so-called Einstein 2E catalog (Harris et al. 1990) that includes only sources above 3.5 σ

Table 2. Summary of IPC sources in the Upper Sco-Cen association

#	RA [J2000]	DEC [J2000]	Rate [10^{-3} cnt/s]	SNR	Offaxis[(1)] [arcmin]	RECO[(2)]	f_X [10^{-14} erg/cm^2/s] [0.2-2.0 keV]	Flag[(3)]
1	15:54:49.4	-23:59:21	3.4	2.7	18.39	400	9.93	Y
2	15:55:00.0	-23:47:13	255.4	40.9	7.34	0	745.77	N
3	15:55:10.2	-23:18:39	4.6	2.9	25.63	0	13.43	Y
4	15:55:21.1	-23:22:03	8.4	5.3	21.85	806	24.53	N
5	15:56:11.7	-23:28:58	5.9	4.5	17.57	804	17.23	Y
6	15:56:12.1	-23:50:09	2.7[(4)]	3.0	11.58	0	10.21	Y
7	15:56:22.8	-23:41:44	2.4[(4)]	2.7	12.03	0	9.07	Y
8	15:56:30.1	-23:47:54	12.1	742	13.83	0	35.33	N
9	15:56:58.6	-23:29:45	4.8	3.2	24.30	1109	14.02	N
10	15:57:20.4	-23:38:26	7.1	4.1	25.73	1006	20.73	N
11	15:57:24.3	-23:54:31	8.9	4.5	28.40	0	25.99	N
12	15:57:34.4	-23:21:59	9.9	3.7	36.19	906	28.91	N
13	16:00:01.0	-22:20:59	17.4	4.6	16.72	100	50.81	N
14	16:00:22.9	-22:37:24	24.8	6.5	1.02	0	72.42	N
15	16:01:06.0	-22:28:00	8.2	3.2	13.81	0	23.94	N
16	16:01:24.3	-22:40:42	24.7	5.7	15.81	0	72.12	N
17	16:02:07.8	-22:55:10	20.1	3.7	30.69	0	58.69	N
18	16:02:11.1	-22:41:15	40.1	6.3	26.11	100	117.09	N

Notes
(1) For the IPC the typical error circle for identification is 50 arcsec, increasing up to 90 arcsec for faint X-ray sources at large offaxis angles (cf. Fig. I.1 of Harris et al. 1990).
(2) The RECO value provides an estimate of the source obscuration due to IPC entrance-window support structure. As shown in appendix A of Micela et al., (1988) the rates of sources with high RECO values are uncertain up to a factor 2.
(3) A value "Y" for this flag indicates that the source is reported here for the first time and has not been listed by WVMBM.
(4) These rates and the corresponding SNR ratios are evaluated in the 0.8-3.5 keV bandpass where these sources have been detected.

another shorter ($\sim$ 3.5 ksec) HRI observation (RH202042n00, PI: Kunkel).

The relative position in the sky of the analyzed X-ray images is shown in Fig. 1 with overlaid the positions of the X-ray sources detected in the pointed observations as well as those listed in the RASS Bright Source Catalog (hereafter RBSC, Voges et al., 1997).

2.1. Detection of X-ray sources in ROSAT images using wavelet transforms

2.1.1. PSPC observation

We have summed up the two segments of the PSPC exposure obtaining a total effective exposure time of 5.2 ksec. In order to account, even in a rough way, for possible temporal variations of X-ray emission, we have decided to analyze both the summed data as well as each of the two time segments separately. The analysis has been performed in the Broad (0.2–2.01 keV), Hard (0.41–2.01 keV) and Soft (0.2–0.41 keV) bandpasses with a detection algorithm recently developed by Damiani et al. (1996a,b; 1997a,b) based on wavelet transforms. This algorithm takes advantage of the information contained in the exposure map and takes into account the variation of the width of the PRF across the entire PSPC field of view. The exposure maps have been computed in each of the above energy bands using the software developed by Snowden and collaborators (Snowden et al., 1994). In order to make the computed maps as good as possible we have computed them as the weighted sum of the seven exposure maps (one for each of the seven sub-bandpasses identified by Snowden and collaborators) using as a weight the X-ray spectrum accumulated over the entire PSPC image and rebinned in the seven energy bandpasses we have considered.

The wavelet transform algorithm allows to detect reliably faint sources in crowded fields or in the presence of a strongly spatially variable background and to assess source intensity, extent and position with their associated uncertainties *directly from the analysis of the wavelet transform of the X-ray image*.

This algorithm has been tested through extensive Monte Carlo simulations in a variety of conditions allowing us to determine the expected number of spurious detections per PSPC image as a function of the threshold probability for source existence. Damiani and collaborators have also shown, that in the case of the PSPC images the number of spurious sources is largely independent from parameters, such as background intensity, number of real sources, etc. In the present analysis of PSPC data we have adopted a probability threshold of 0.99325 (i.e. a single-side gaussian probability level of 4.3 σ) resulting in no more than 1 expected spurious detection. In Table 3 we

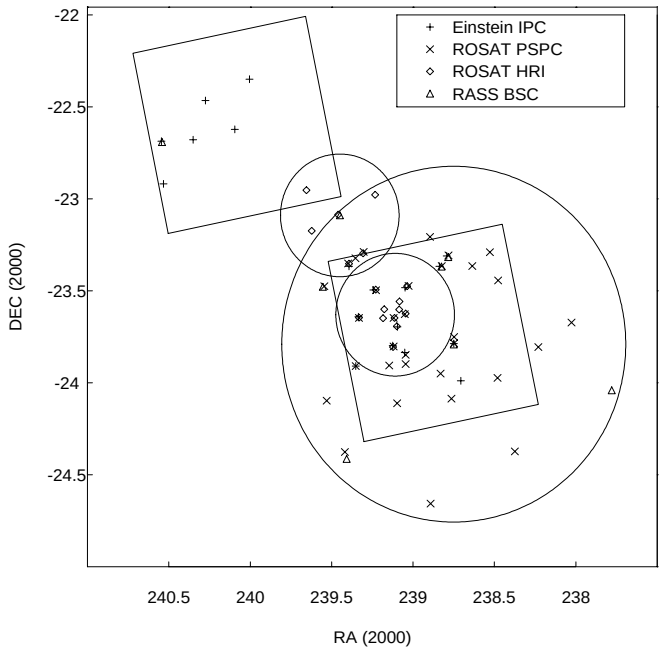

Fig. 1. Schematic representation of the relative positions of the studied X-ray images and of detected X-ray sources. The big circle indicates the PSPC field-of-view (FOV), the two small circles schematically represent the FOV of the two HRI observations, and the two squares the FOV of the two IPC observations. Sources detected with different instruments are indicated with different symbols.

list the positions of PSPC detections, with their 90% uncertainty radius which gives a good estimate of the size of the sky region that should be searched for optical counterparts. We report also an estimate of source extent with respect to the local width of the instrument PSF (cf. note to Table 3). Since the computed extent ranges by a factor of 2 around 1 (the nominal value for point-like sources) we conclude that all PSPC sources are consistent with being point-like (cf. Damiani et al., 1997b). The standard SASS processing of the two segments has detected in the [0.2-2.4 keV] band-pass a total of 16 distinct sources, 7 of which have been detected in both the two segments and 13 are in common with the 32 sources we have detected with the wavelet transform analysis. The large improvement of our PSPC detection code with respect to the SASS one is clearly evident.

Given our lack of knowledge on individual source absorption and temperature the conversion factor from count-rate to flux has been evaluated for the same ranges of log N_H and temperatures as for the IPC sources. The adopted conversion factors are 1.472 10^{-11} ($\pm$53%) and 9.904 10^{-12} ($\pm$26%) erg cm^{-2} cnt^{-1} for rates in the PSPC (0.2-2.01 keV) and (0.42-2.01 keV) energy bands, respectively, where the error reflects the range of admissible temperature and absorption values. Again the uncertainties in the adopted conversion factors largely dominate the error on the source flux.

2.1.2. HRI observations

A similar analysis but with a slightly different wavelet transform detection algorithm to account for the specific properties of the ROSAT HRI (cf. David et al., 1993) has been applied to the two HRI observations. The deeper observation is affected by the presence of a hot spot in the lower left corner of the HRI image. The hot spot produces two evidently spurious detections which were removed to produce the final list of 11 detections, whose properties are summarized in the upper part of Table 4. The entries in the lower part of the same table summarize the properties of the 6 sources detected in the shorter HRI observation.

The number of spurious sources in an HRI image is not only a function of the adopted source acceptance threshold but it also depends on the overall image background, which roughly increases with the exposure time (Damiani et al., in prep). To have no more than a single spurious detection in each image we have to adopt a probability threshold of 4.6 σ for images of about 30 ksec, and of 4.45 σ for images of about 3 ksec[2]. With this choice we expect less than one spurious detection in each HRI image. Moreover since all detections are well above the chosen confidence level we are confident that they are all "statistically" real. However, since the ROSAT HRI suffers an UV-leak (cf. David et al., 1993), whose likely origin has been only recently understood as an excess filter trasmissivity mainly in the 2000–3000 Å bandpass (Barbera et al., 1997; Zombeck et al., 1997), we have taken advantage of the limited spectral capability of the HRI in an attempt to discriminate the true X-ray sources from those sources likely due to UV contaminating emission. These latter sources would show an HRI pulse-height spectrum with a peak in the two lowest channels. On the contrary typical X-ray sources and especially those associated with emitters in the Upper Sco Cen association, seen through a column of interstellar matter with Log (N_H) $\geq$ 20.2 cm^{-2}, should show a peak in the HRI channels from 5 to 7. As a result of the analysis of the HRI spectra and taking into account the limited statistics, we have found that none of the HRI sources are affected by the UV-leak, i.e. their spectra show a peak in channels 6-7, consistent with the emission being truly due to X-rays. Finally we note that, similarly to the PSPC case, all HRI sources have extent that are consistent with their being point-like. The HRI SASS processing has detected a total of 17 HRI sources (eliminating those clearly associated with the hot spots), 15 of them being in common with those found by the detection algorithm we have adopted.

The adopted conversion factor from HRI count rate to X-ray flux is 3.745 10^{-11} ($\pm$55%) erg cm^{-2} cnt^{-1}. Again the uncertainty is due to the range of admissible temperature and absorption and dominates other errors even for the weakest source.

[2] Since the number of spurious detections is quite a strong function of the value of acceptance threshold, even such a small difference in the threshold produces a significant difference in the expected number of spurious detections

Table 3. Summary of PSPC detections

#	RA [J2000]	DEC [J2000]	P-co[(1)]	Rate [10^{-3} cnt/s]	Error	Prob. of[(2)] Existence	Source[(3)] Extent	Offaxis [']	R-co[(4)]	r_{90}[(5)] ["]	f_X [10^{-14} erg/cm^2/s] [0.2-2.0 keV]
1	15:52:06.4	-23:40:19	2h	30.74	9.55	4.7	1.4	40.4	2b	156.4	45.31
2	15:52:55.4	-23:48:21	1s	11.65	4.40	4.5	1.6	28.5	1s	103.6	—[(6)]
3	15:53:30.0	-24:22:23	Sh	23.32	7.27	4.6	1.5	40.6	Sb	161.1	34.37
4	15:53:54.6	-23:26:39	1h	10.29	5.60	4.9	0.5	25.6	1h	82.2	10.19
5	15:53:55.5	-23:58:24	Sh	18.63	2.99	12.4	1.0	18.4	Sb	29.9	27.46
6	15:54:06.7	-23:17:24	Sh	41.90	5.09	14.4	1.1	32.4	Sb	53.5	61.76
7	15:54:32.8	-23:21:54	2b	5.52	2.11	4.7	0.5	26.3	2b	88.4	8.14
8	15:54:59.5	-23:47:10	Sh	584.83	10.82	111.9	0.8	0.3	Sb	14.0	862.4
9	15:54:59.5	-23:45:02	Sh	11.32	1.65	12.9	0.7	2.4	Sb	17.5	16.69
10	15:55:03.3	-24:05:10	Sh	6.23	2.28	4.5	1.6	17.8	Sh	59.1	6.17
11	15:55:07.7	-23:18:25	Sh	17.25	4.29	10.8	0.6	29.1	Sb	52.6	25.43
12	15:55:17.5	-23:21:55	Sh	144.78	7.24	46.1	0.9	25.8	Sb	31.8	213.41
13	15:55:19.2	-23:57:02	Sh	1.92	0.84	4.3	0.7	10.6	Sh	42.5	1.90
14	15:55:34.1	-24:39:24	Sh	47.93	9.10	5.7	1.2	52.6	Sb	181.2	70.65
15	15:55:34.9	-23:12:24	Sh	35.80	6.38	10.6	1.0	35.9	Sb	69.8	52.77
16	15:56:06.5	-23:28:24	Sh	17.53	4.76	7.2	1.5	24.4	Sb	54.2	25.84
17	15:56:11.1	-23:53:54	Sh	6.99	2.18	6.9	0.7	17.5	Sb	39.1	10.30
18	15:56:11.1	-23:50:54	Sh	4.83	1.76	6.3	0.6	16.6	Sb	39.9	7.12
19	15:56:12.1	-23:37:39	Sh	4.60	1.74	4.7	0.7	19.2	Sb	61.0	6.78
20	15:56:23.3	-24:06:38	1h	12.39	4.51	5.0	0.9	27.0	1h	84.7	12.27
21	15:56:28.5	-23:38:53	Sh	11.38	3.33	7.4	0.8	22.0	Sb	47.2	16.77
22	15:56:28.6	-23:48:08	Sh	20.13	5.16	11.2	0.9	20.3	Sb	34.3	29.67
23	15:56:35.2	-23:54:23	Sb	5.10	1.90	4.3	0.8	22.8	Sb	82.0	7.52
24	15:56:54.5	-23:29:52	Sh	7.74	2.61	5.0	0.8	31.5	Sh	104.8	7.67
25	15:57:12.8	-23:17:21	2h	14.98	17.65	4.5	0.7	42.8	2h	178.0	14.84
26	15:57:19.8	-23:38:51	Sh	11.72	3.42	6.3	0.7	33.1	Sb	88.3	17.28
27	15:57:24.4	-23:54:35	Sh	24.86	6.57	7.0	1.4	33.8	Sb	83.5	36.64
28	15:57:24.9	-23:19:20	Sb	30.88	8.73	5.6	1.4	43.5	Sb	142.4	45.52
29	15:57:35.8	-23:21:05	Sh	15.91	4.66	6.1	0.7	44.4	Sh	135.2	15.76
30	15:57:40.3	-24:22:34	Sh	43.29	10.94	7.2	1.1	50.7	Sb	141.7	63.81
31	15:58:07.3	-24:05:47	Sh	44.09	7.01	10.5	0.9	46.6	Sb	99.6	64.99
32	15:58:10.8	-23:28:32	Sh	160.69	10.45	27.2	1.1	47.6	Sb	75.1	236.86

Notes

(1) This code gives the derivation of positions: the first letter indicates if the RA and Dec have been evaluated in the summed image (S), in the first (1), or in the second (2) segment, the second letter indicates the energy band (h=Hard, s=Soft, b=Broad). Given the PSPC properties we have given preference whenever possible to positions determined in the Hard band.

(2) Source probability of existence, expressed as the number of standard deviations of a single-side gaussian distrubution integral.

(3) The extent is normalized to the PSF sigma computed at the source offaxis angle following Hasinger et al. (1993a). The PSF is computed at an "effective" energy of 0.3 keV that yields a good approximation of the real PSF for sources over an ample range of spectral parameters and absorption values (cf. Damiani et al., 1997b).

(4) This code gives the derivation of source intensity, associated errors, and source significance. The coding scheme is analogous to that described in note (1). In this case, however, the precedence has been given to quantities evaluated in the broad band.

(5) The 90% error circle has been computed according to the analytical formulation derived by Damiani et al. (1997b), i.e. $r_{90\%} = \sigma_{psf} * 0.525 * \exp(5.433/n_{sigma})$ where σ_{psf} is the width (standard deviation) of the gaussian component of the PSF computed as a function of off-axis angle according to Hasinger et al. (1993a) and n_{sigma} is the source probability of existence expressed as the number of standard deviations of a gaussian distribution. In this case an energy of 0.3 keV has been adopted to evaluate the PSF. A further additional uncertainty of 10 arcsec has been added in quadrature to account for the known limitation of the absolute aspect reconstruction of the ROSAT satellite.

(6) Source 2 has been detected only in the soft bandpass and therefore it is likely to belong to a different class of objects than the rest of sources and to be subject to a quite different interstellar absorption. Lacking further information on its nature we have decided to not compute the flux for this source.

Table 4. Summary of HRI detections

#	RA [J2000]	DEC [J2000]	Rate [10^{-3} cnt/s]	Error	Prob. of[(1)] Existence	Source[(2)] Extent	Offaxis [']	r_{90}[(3)] ["]	f_X [10^{-14} erg/cm^2/s] [0.2-2.0 keV]
1	15:56:08.8	-23:28:28	3.089	0.39	14.7	0.84	10.2	11.1	11.57
2	15:56:10.9	-23:37:28	0.834	0.26	6.1	1.38	3.6	10.4	3.12
3	15:56:19.9	-23:33:31	0.936	0.30	5.5	1.96	4.6	10.6	3.51
4	15:56:20.6	-23:36:06	1.344	0.25	10.3	1.01	2.2	10.1	5.03
5	15:56:23.9	-23:41:33	1.409	0.27	9.6	1.31	3.8	10.2	5.28
6	15:56:27.5	-23:38:48	3.177	0.36	16.9	1.33	1.0	10.1	11.90
7	15:56:29.3	-23:48:21	6.985	0.59	24.3	0.85	10.5	10.9	26.16
8	15:56:42.6	-23:36:00	0.497	0.19	4.8	0.98	4.1	10.6	1.86
9	15:56:44.2	-23:38:55	1.233	0.24	10.8	0.80	4.2	10.2	4.62
10	15:56:54.9	-23:29:40	3.074	0.41	13.8	0.83	10.4	11.2	11.51
11	15:57:20.1	-23:38:47	5.735	0.54	21.1	0.83	12.2	11.6	21.48
12	15:56:55.7	-22:58:41	9.137	2.65	9.3	0.7	13.8	14.5	34.22
13	15:57:13.7	-23:17:46	6.734	2.17	5.9	0.9	14.7	19.4	25.22
14	15:57:34.4	-23:21:12	8.637	2.71	7.0	0.8	16.1	20.2	32.35
15	15:57:50.2	-23:05:09	5.854	1.67	9.5	1.0	0.5	10.1	21.92
16	15:58:29.5	-23:10:26	2.201	1.08	5.0	0.4	10.7	14.6	8.24
17	15:58:37.0	-22:57:11	12.501	2.31	11.1	0.7	14.0	13.9	46.82

(1) Source probability of existence expressed as the number of standard deviation such that the single-side gaussian integral results in the same probability level.
(2) Sources extension is evaluated in units of the width of the HRI PSF at source position. The width is expressed, in the approximation of a gaussian PSF, as $\sigma = R_{HP}/\sqrt{2 * \ln(2)}$, where the expression for the half-power radius, R_{HP} and its dependence from the offaxis angle is given by David et al. (1993).
(3) The radius of the error circle on X-ray position is based on the same relation discussed in the case of the PSPC (cf. note 5 to Table 3). Given the known, yet unexplained, limitation of the ROSAT aspect reconstruction (David et al. 1993, Briel et al. 1996) we have added in quadrature a further uncertainty of 10 arcsec to the formally derived 90% radius.

2.2. Comparison among X-ray observations

2.2.1. PSPC and HRI observations

A positional cross-matching of the PSPC and HRI detections (cf. Fig. 1 and Table 5) shows that 8 HRI sources have been also detected with the PSPC. While the adopted matching radius was 1 arcmin, the positional offsets among the PSPC and the HRI positions is usually less than 20 arcsec and in no case greater than 35 arcsec. 21 PSPC sources fall outside the two HRI images. For the remaining 4 PSPC sources falling in the combined HRI field-of-view we have evaluated the upper limits to the HRI flux that in three cases are consistent with the measured PSPC flux, while in the case of the source USco-036 the value of upper limits is log $L_X < 29.74$ erg s^{-1} a factor 2.5 below the luminosity (log L_X = 30.15 erg s^{-1}) measured with the PSPC. Among the nine additional HRI sources, three fall outside the PSPC field-of-view, the remaining six HRI sources fall in regions where the HRI is more sensitive than the PSPC. In the case of source USco-032 the derived PSPC upper limit is marginally compatible with the deduced HRI rate. A more detailed discussion on the issue of long-term variability is deferred to Sect. 4.

2.2.2. ROSAT pointed data and Einstein data

We have also matched our list of ROSAT X-ray sources with the list of IPC sources of Table 2. Adopting a positional matching radius of 1 arcmin we have found that 11 out of the 18 IPC sources have also been detected with the PSPC or the HRI, specifically 5 with the PSPC only, 5 with both the PSPC and the HRI, and 1 with the HRI only. It is noteworthy that 4 out of the 5 weak IPC sources we report here for the first time are also confirmed by the new ROSAT observations. For the weak source (the first listed in Table 2) that has not been confirmed we have computed an upper limit to the PSPC flux half a order of magnitude below the flux measured with the IPC. However it is possible that this source is spurious. The other seven IPC sources fall outside the region surveyed with the pointed ROSAT observations.

2.2.3. Pointed data and RASS bright sources

Five PSPC, 1 HRI and 6 IPC sources have been cross-matched with 9 distinct sources in the RBSC (Voges et al., 1997). Two additional RBSC sources fall in the region of the sky we have

Table 5. List of X-ray sources detected in the present survey with different instruments and their cross-matching

			PSPC			HRI			IPC			RBSC		
Src	RA	DEC	#	Δ	Log $L_X^{(1)}$	#	Δ	Log L_X	#	Δ	Log L_X	1RSX	Δ	Log $L_X^{(2)}$
	[J2000]	[J2000]		["]	[erg/s]		["]	[erg/s]		["]	[erg/s]		["]	[erg/s]
1	15:51:07.1	-24:02:25			<29.93							J155107.1-240225	0.0	30.34(20%)
2	15:52:06.4	-23:40:19	1	0.0	30.14		–							
3	15:52:55.4	-23:48:21	2	0.0	–		–							
4	15:53:30.0	-24:22:23	3	0.0	30.02		–							
5	15:53:54.6	-23:26:39	4	0.0	29.50		–				<29.61			
6	15:53:55.5	-23:58:24	5	0.0	29.93		–				<29.53			
7	15:54:06.7	-23:17:24	6	0.0	30.28		–				<29.68			
8	15:54:32.8	-23:21:54	7	0.0	29.40		–				<29.50			
9	15:54:49.4	-23:59:21			<29.00				1	0.0	29.48			
10	15:54:59.5	-23:47:10	8	0.0	31.42		–		2	8.4	31.36	J155500.0-234729	20.9	31.14(11%)
11	15:54:59.5	-23:45:02	9	0.0	29.71		–				<29.44			
12	15:55:03.3	-24:05:10	10	0.0	29.28		–				<29.44			
13	15:55:07.7	-23:18:25	11	0.0	29.89		–		3	40.1	29.62	J155508.9-231859	34.8	30.38(24%)
14	15:55:17.5	-23:21:55	12	0.0	30.82		–		4	54.7	29.88	J155518.0-232205	12.9	30.42(23%)
15	15:55:19.2	-23:57:02	13	0.0	28.77		–				<29.46			
16	15:55:34.1	-24:39:24	14	0.0	30.44		–							
17	15:55:34.9	-23:12:24	15	0.0	30.21		–				<29.63			
18	15:56:08.8	-23:28:28	16	34.8	29.90	1	0.0	29.55	5	52.9	29.72			
19	15:56:10.9	-23:37:28	19	20.8	29.32	2	0.0	28.98						
20	15:56:11.1	-23:53:54	17	0.0	29.50			<29.41			<29.47			
21	15:56:11.1	-23:50:54	18	0.0	29.34			<29.20	6	47.3	29.50			
22	15:56:19.9	-23:33:31			<29.30	3	0.0	29.03			<29.48			
23	15:56:20.6	-23:36:06			<29.36	4	0.0	29.19			<29.46			
24	15:56:23.3	-24:06:38	20	0.0	29.58		–				<29.52			
25	15:56:23.9	-23:41:33			<29.26	5	0.0	29.21	7	19.9	29.45			
26	15:56:27.5	-23:38:48	21	15.6	29.71	6	0.0	29.56						
27	15:56:29.3	-23:48:21	22	16.4	29.96	7	0.0	29.90	8	28.7	30.04			
28	15:56:35.2	-23:54:23	23	0.0	29.36			<29.41			<29.49			
29	15:56:42.6	-23:36:00			<29.34	8	0.0	28.76			<29.49			
30	15:56:44.2	-23:38:55			<29.30	9	0.0	29.15			<29.48			
31	15:56:54.9	-23:29:40	24	13.1	29.54	10	0.0	29.55	9	55.7	29.63			
32	15:56:55.7	-22:58:41			<29.95	12	0.0	30.02						
33	15:57:13.7	-23:17:46	25	28.7	29.66	13	0.0	29.89						
34	15:57:20.1	-23:38:47	26	6.0	29.72	11	0.0	29.82	10	21.5	29.80			
35	15:57:24.4	-23:54:35	27	0.0	30.05		–		11	5.0	29.90			
36	15:57:24.9	-23:19:20	28	0.0	30.15			<29.74			<29.71			
37	15:57:34.4	-23:21:12	29	22.3	29.68	14	0.0	30.00	12	47.2	29.95			
38	15:57:38	-24:24:47	30	137.2	30.29		–					J155738.6-242448	0.0	30.33(23%)
39	15:57:50.2	-23:05:09		–		15	0.0	29.83				J155748.8-230521	35.2	30.40(20%)
40	15:58:07.3	-24:05:47	31	0.0	30.30		–							
41	15:58:10.8	-23:28:32	32	0.0	30.86		–					J155813.2-232841	34.2	30.45(19%)
42	15:58:29.5	-23:10:26		–		16	0.0	29.40			<30.06			
43	15:58:37.0	-22:57:11		–		17	0.0	30.16			<29.98			
44	16:00:01.0	-22:20:59		–					13	0.0	30.19			
45	16:00:22.9	-22:37:24		–			–		14	0.0	30.35	J160018.3-223707	75.4	30.25(26%)
46	16:01:06.0	-22:28:00		–					15	0.0	29.87			
47	16:01:26.1	-22:40:47		–			–		16	25.9	30.35	J160126.1-224047	0.0	30.39(21%)
48	16:02:00.7	-22:21:33		–							<29.87	J160200.7-222133	0.0	30.29(24%)
49	16:02:07.8	-22:55:10		–					17	0.0	30.26			
50	16:02:10.1	-22:41:28		–			–		18	20.8	30.56	J160210.1-224128	0.0	30.45(19%)

Notes:
(1) The X-ray luminosity is given in the [0.2-2.01 keV] bandpass and for a distance of 160 pc.
(2) The percentage error quoted in the RSBC is indicated in parentheses.

explored (cf. Fig. 1) and they have been added to our final list of X-ray sources.

As a result of this analysis we have a list of 50 X-ray sources, 33 of which have been detected for the first time in the three pointed ROSAT observations or in the two IPC images we have analyzed. The complete list is summarized in Table 5, where we report the adopted position, the running number in the PSPC, HRI, and IPC tables, the offset, Δ (in arcsec), between the adopted position (preference has been given to positions with the smallest uncertainties) and those measured with the other detectors. We list also the X-ray luminosity of sources for an adopted distance of 160 pc (the distance of the Upper Sco-Cen association). In Table 5 we report also the upper limit we have computed with the PSPC at the position of 1RSX-J155107.1-240225 and with the IPC at the position of 1RSX-J160200.7-222133.

3. The Log N – Log S in the surveyed Upper Sco-Cen region

To put on a more quantitative base our finding of a substantially large number of sources weaker than those previously reported we have built the Log N – Log S (cf. Fig. 2) derived from the IPC results (including also the weaker sources, not reported by WVMBM) and have compared it with the Log N – Log S we have derived from the analysis of the PSPC and HRI observations. In order to derive the Log N – Log S we have used the sensitivity maps evaluated with the wavelet transform detection algorithm (Damiani et al., 1997a; Damiani et al., 1997b) for the PSPC and HRI observations and that computed according to Harris et al. (1990) for the IPC. In deriving the ROSAT Log N – Log S we have assigned a unique flux value to each of the 40 distinct sources, adopting the mean flux for the eight sources seen with both the HRI and the PSPS at a similar flux level.

For fluxes greater than 10^{-13} erg cm^{-2} s^{-1} the *"Einstein"* and the "ROSAT" Log N – Log S are in very good agreement (especially taking into account the difficulties in cross-calibrating two instruments with different band-passes).[3] Both Log N - Log S diagrams, especially the one from ROSAT data, show that the number of sources continues to increase (with a slope of approximately 1.5) toward weak fluxes and indicates the incompleteness of the sample of the sources detected with the *Einstein* IPC.

In order to understand the possible nature of the population of the weaker sources we have computed the predicted Log N – Log S for the "normal" stellar population of coronal emitters in the Galaxy toward the explored region using the latest version of the so-called XCOUNT model (Favata et al., 1992; Sciortino et al., 1995). This model takes into account the influence of stellar age on the intensity and spectra of X-ray coronal emission for age ranging from 10^7 (very young disk population) to 10^{10} years (old disk population), the effect of X-ray unresolved binaries, and the effect of interstellar absorption. In performing all calculations we have assumed a constant stellar birthrate that has been shown to be in good agreement with the observed stellar content of the Extended Medium Sensitivity Survey (Micela et al., 1993). Our model calculation shows that the "normal" stellar population, including the population of active binaries, at the galactic latitude of Upper Sco-Cen (b $\sim 23^\circ$) contributes approximately only 1/50 to the observed source population. It is worth to notice that a similar result would have been obtained also with the model recently presented by Guillolt et al. (1996). Furthermore we have evaluated the expected contamination of our survey from extragalactic sources. Based on the Log N – Log S derived by Hasinger et al., (1993b) and Branduardi-Raymont et al. 1994, and assuming that the emisson of all extragalactic source can be modeled with a power law with index, α, in the range 1–2 seen through an hydrogen column with log N$_H \sim 21.1$ (as derived from the HI survey data of Stark et al. (1992)) we have computed that our survey contains less than 7–8 extragalactic sources. Taken at face value all these results strongly suggest that *most of the sources we have detected must belong to a localized population of likely PMS stars in the Upper Sco-Cen association.*

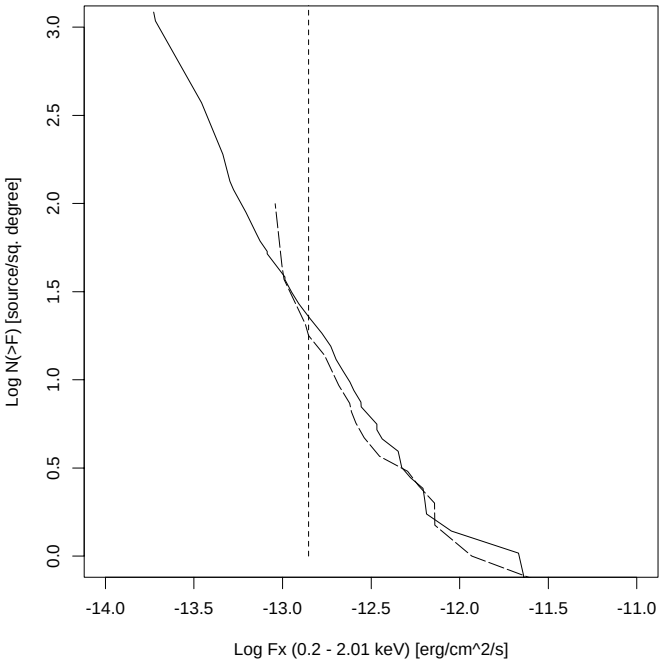

Fig. 2. The Log N - Log S deduced from the sample of sources detected with the pointed ROSAT observations (solid line) and with the Einstein IPC (long-dashed line). The vertical line marks the flux of the weakest IPC source reported by WVMBM. Note that the larger size of the ROSAT source sample allows us to better define the shape of the Log N – Log S, in particular below the limit of the WVMBM survey. Since the Log N – Log S does not seem to flatten at weaker flux, the total number of X-ray emitters, most of which are likely associated with stars of the Upper Sco association, is significantly greater than that obtained with the IPC and reported by WVMBM.

[3] The more rapid increase of the *Einstein* Log N – Log S just below the WVMBM limiting sensitivity is likely due to the extremely small number of IPC sources involved, making noisy the computed Log N – Log S.

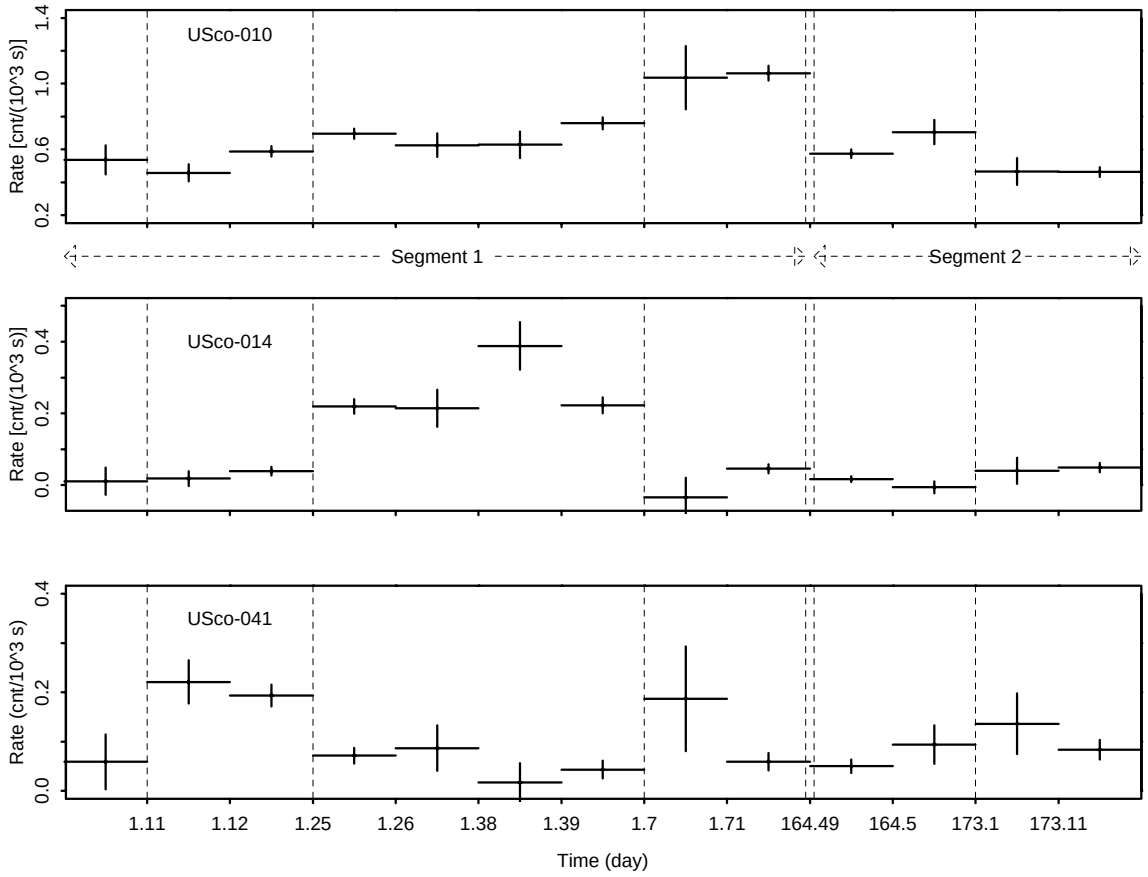

Fig. 3. Light curves for the three PSPC sources where variability on time scale of hours or days is present. The vertical dashed lines mark the separation among the various sub-segments of the observations. The double dashed vertical line marks the separation among segments 1 and 2. Notice that data of segment 1 have been collected along two days, while those of segment 2 (taken six month later) span about ten days.

4. Variability and spectra

4.1. Short-term variability

We have searched the PSPC and HRI sources for variability using the Kolmogorov-Smirnov (KS) and the Cramer-vonMises (CvM) tests as implemented in the task "vartst" available in PROS V2.10.2. We have analyzed each data segment, separately (for a combined analysis of the two PSPC segments see below). Variability with statistical significance above 99% (in both tests) has been detected with the PSPC in segment 1 for source USco-014 and in segment 2 for sources USco-010, USco-014 and USco-041. In order to verify that these results are not affected by the presence of variability in the background level we have constructed for these three PSPC sources the background-subtracted light-curves shown in Fig. 3. These light-curves confirm the existence of variability on time scales of fraction of days, that are typical of intense flares, even if it is unclear if all the observed variability can be explained in terms of the occurence of flares. It is worth noting that flares with similar intensity have been reported in Pleiades M stars (Sciortino et al., 1994, Micela et al., 1995, Gagné et al., 1995a), in Orion late-type stars (Gagné et al., 1995b) and in NGC1333 PMS stars (Preibisch, 1997a). However the flare we observe are not as large as those seen on some other PMS stars (e.g. Montmerle et al., 1983; Preibisch et al., 1993; Preibisch et al., 1995; Carkner et al., 1996; Grosso et al., 1997).

For all the HRI sources it is not possible to reject, above the 99% confidence level, the hypothesis of the sources being constant. This is not surprising given the small number of counts for each source.

4.2. Six-month variability

We have taken advantage of the six month separation between the two segments of the PSPC observation to explore the variability on this time scale. In performing this analysis we have considered only the sources detected in at least one of the two segments; this requirement excludes two sources that have been detected only in the summed data. Furthermore we have excluded the source detected only in the soft band, since its nature is likely different from that of the rest of the source population. We have constructed the Maximum Likelihood (ML) variability distribution (cf. Sciortino & Micela, 1992; Schmitt et al., 1993) for the ratio of count rates measured in the second, shorter segment versus those measured in the first,

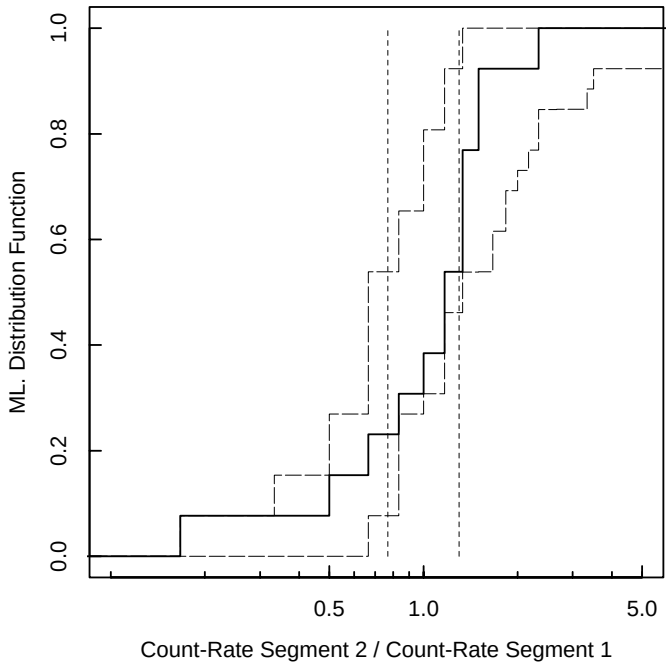

Fig. 4. The Maximum Likelihood variability distribution for the 28 PSPC sources we have retained in our variability analysis on six-month time-scale (solid line).The two long-dashed lines show the 99% range for the cumulative ML variability distribution obtained through 200 Monte Carlo simulations based on the bootstrap technique. The two vertical short-dashed lines indicate variations of 30%.

longer segment. If a source has not been detected in one of the segments we have evaluated the upper limit to its count-rate with the same wavelet transform method we have used for the detections (cf. Damiani et al. 1997a,b), i.e. all count rates have been derived in an uniform and self-consistent way. The derived ML variability distribution is shown as a solid line in Fig. 4. This distribution shows that about 20-25% of the sources varies more than a factor of 2 (the fraction being almost equally divided between the two tails of the distribution). To address the question of the statistical significance of this result we have generated via Monte Carlo simulations 200 sets of count-rate ratios, by randomly extracting count-rates for detections from a normal distribution having mean and variance equal to the measured rate and associated error of each source, respectively, and keeping unchanged the values for the upper-limits as those derived from the real data. After having computed the 200 ML variability distributions we have derived for each bin of the rate ratio the 0.5% and 99.5% quantiles of the distributions. The resulting "minimum" and "maximum" variability distributions are shown as the long-dashed lines in Fig. 4. In summary, when one includes the effect of counting statistics (i.e. one accounts for the rate uncertainties) the data are compatible with 0% to 50% of sources varying more than a factor of two, while for smaller amplitude variations (let say of 30%, shown in Fig. 4) the fraction of variable sources is in the 20% to 100% range.

The fraction of the sources in the present survey that vary more than a factor 2 on a sixth month time-scale is comparable to the fraction of Pleiades stars that, on similar time-scales, have varied by a factor 2 (Sciortino et al., 1994; Micela et al., 1995; Gagné et al., 1995a) and to the fraction of Orion X-ray emitting members that have varied above the 3σ level on a time scale of 1 yr (Gagné et al., 1995b).

4.3. Long-term variability

As mentioned above the conversion from measured rate to source intrinsic flux is subject to uncertainty up to 50% due to the (unknown) intrinsic source specrum and line-of-sight absorption. Since the largest statistical (counting) error among the weak sources we have detected is $\sim$ 40%, usually the uncertainty in the conversion factor is the most stringent limit on our ability to assign an X-ray flux to each individual source. However if one is interested only to compare the fluxes derived from different instruments *for the same source* the associated uncertainty in the comparison is smaller. Indeed for a given (i-th) source the ratio of two X-ray fluxes deduced from the rates, $\mathrm{I}_{i,A}$ and $\mathrm{I}_{i,B}$, measured with instruments A and B is

$$\mathrm{F_{i,A}/F_{i,B}} = \mathrm{cv_A/cv_B} * \mathrm{I_{i,A}/I_{i,B}}, \quad (1)$$

where $\mathrm{cv_A}$, $\mathrm{cv_B}$ are the conversion factors for instruments A and B, respectively. Given the above expression it is clear that our ability to detect significant long-term variability on source i-th is limited 1) by the counting statistics, that is reflected by the error on rates, I_i, and 2) by the additional uncertainties in the ratio $\mathrm{cv}_A/\mathrm{cv}_B$, due to the source emission model assumed in computing the conversion factors. For the Raymond-Smith single temperature plus absorption model and the (ample) ranges of temperature and N_H we have explored (cf. Sect. 2) and under the hypotheses that both coronal temperature and absorption of a given source do not vary these uncertainties are at most $\pm$ 3%, $\pm$ 12% and $\pm$ 12%, for the PSPC-HRI, the PSPC-IPC and the HRI-IPC comparisons, respectively. These uncertainties increase at most to $\pm$ 25% for all three pairs of instruments if we allow the temperature to vary in the 0.5-1.3 keV range (as it could occur during a stellar flare) between the two observations for a fixed value of N_H.

The above reasoning makes it possible to separate the effect due to the counting statistic uncertainties from those due to our ignorance on source intrinsic spectra. Hence we can conclude that variations greater than the above limits should be explained with counting statistic errors or should be interpreted as evidence of variation, in spectrum and/or in intensity, of X-ray emission.

In Fig. 5 we have summarized all the available variability data. If we adopt as criterion for variability the condition that the 2σ error bars do not intersect the "non-variability" regions enclosed by the dotted (or dashed) lines we find that in comparing PSPC and HRI fluxes as well as IPC and HRI fluxes no sources show up as variable. In the case of the PSPC-IPC comparison (i.e. on 12 year time scale) the source USco-011 is variable above the 2σ level and sources USco-006, USco-007, USco-014, USco-017 even considering the 3σ level. However since the source USco-014 (the only being detected both with

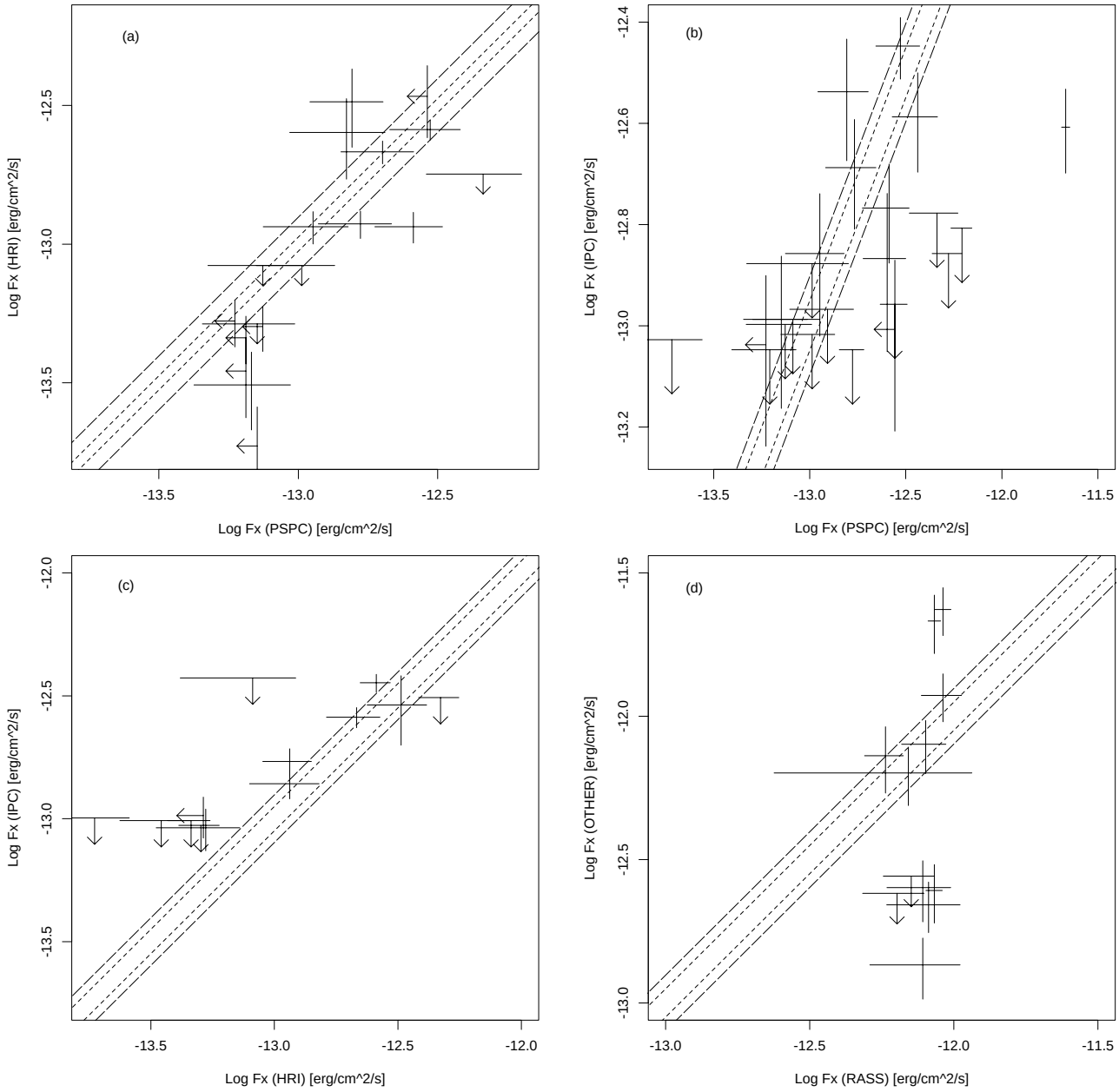

Fig. 5a–d. Scatter plots of fluxes measured with two distinct instruments. All points consisting of a pair of upper limits have not been shown to simplify the appearance and readability of the plots. In panel (a) we compare the flux measured with the PSPC and the HRI. All points are shown with their associated statistical (counting) 1-σ error bars. The short-dashed lines define the admissible range for a source of unchanging intensity, spectrum and absorption, while the long-dashed lines correspond to sources of constant intensity and absorption, but whose temperature has changed within the range we have considered (see text). Any object whose error bars does not reach one of the two long-dashed lines is likely to have varied either in intensity and/or spectrum, while sources falling between the first and the second pairs of lines are likely to have varied their X-ray spectra even if their emission has a nearly constant broad-band intensity. In panel (b) we show an analogous scatter plot, but for the PSPC-IPC case, in panel (c) for the HRI-IPC case, in panel (d) we compare the RBSC derived fluxed with those derived by all other available measurements.

the PSPC and the IPC) is partially obscured in the IPC observation its variability could be suspicious. Finally the comparison of the RBSC fluxes with those deduced by the pointed observations results in 5 sources: USco-001, USco-013, USco-014, USco-039, USco-048, fulfilling the 2σ criterion, and only 1 of them: USco-014 fulfills the 3σ criterion. It is worth to note that the source USco-013 has a RBSC flux significantly different from both that measured with the IPC and a pointed PSPC observation, while these latter two values are compatible with the source being constant.

The results of the above analysis are not completely conclusive since significant variability is not present in all the four intercomparisons, and it is always difficult to account for possible systematic effects in comparing different instruments. However, assuming that the systematic effects are not dominating the IPC-PSPC comparison (i.e. in the case of the two instruments with the smallest counting uncertanties), we can conclude that a clear indication of significant variability on time scale of a decade, i.e. on the time scale of solar magnetic activity, is present in our data. A similar result has also been obtained by the comparative analysis of IPC and PSPC data of Pleiades members (Sciortino et al., 1994; Micela et al., 1995; Gagné et al., 1995b).

4.4. Analysis of PSPC spectra

Three of the PSPC sources are strong enough to make it possible to accumulate spectra with more than 300 net counts during the entire observation. In order to characterize the spectral properties of these sources we have performed simple fits of the observed PSPC spectra with a model of optically thin single temperature emitting plasma with abundance fixed to the solar value leaving the plasma temperature, the column hydrogen column and the overall source flux (i.e. the normalization) as free parameters. All fits have been performed with XSPEC adopting the Raymond-Smith plasma emission model and including the PSPC channels from 4 to 32. The result of these fits are summarized in Table 6 together with the double temperature fit we have performed for the source USco-010 whose spectrum cannot be fitted with the simple 1-T model. The observed spectra and model fits for USco-010, and for USco-041 are shown in Fig. 6.

The results of the fits shows that in all cases most of the emitting plasma has a temperature near to 1 keV and that the source column hydrogen density ranges from $\sim 3\ 10^{20}$ up to 10^{21} cm^{-2}. Given the observed fact that, over an ample range of stellar activity levels and ages, stellar coronal spectra become softer with increasing stellar age and/or decreasing stellar activity level (Vaiana, 1983; Micela, 1991; Gagné et al., 1995b; Preibisch, (1997b); Micela et al., 1997) the spectra we have studied are compatible with the sources being stars of a young or PMS population, and indeed the counterparts (cf. Sect. 5) of sources USco-010 and USco-014 are two PMS stars showing strong lithium absorption according to WVMBM.

In order to investigate the spectral properties of the weak sources and to compare them to those of the sources for which

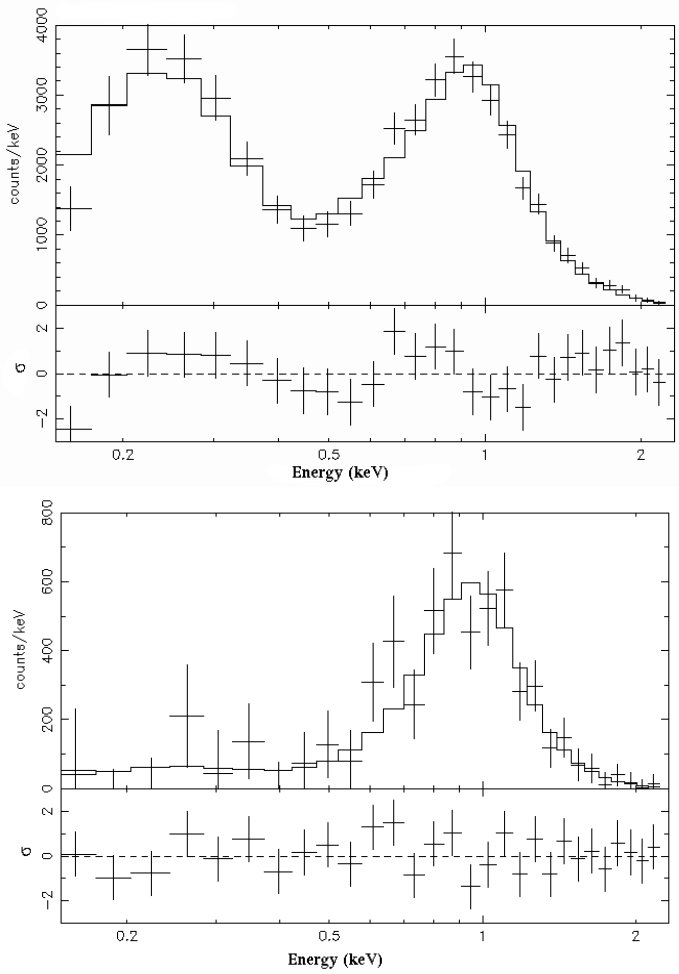

Fig. 6. [upper panel] The observed PSPC spectrum and the two-temperature model fit for the source USco-010. The bottom part of the figure shows the residuals between the observed and the fitted spectra expressed in term of the number of standard deviations of measured counts in each channel. [lower panel] The observed spectrum and the single-temperature fit for the source USco-041. Bottom part of the figure as in the upper panel.

we have performed spectral fits we have computed for all the 24 PSPC sources detected in the broad band the hardness ratios

$$HR_1 = (\sum_{3}^{10} C_i - \sum_{13}^{30} C_i)/(\sum_{3}^{10} C_i + \sum_{13}^{30} C_i), \text{ and}$$

$$HR_2 = (\sum_{13}^{18} C_i - \sum_{19}^{30} C_i)/(\sum_{13}^{18} C_i + \sum_{19}^{30} C_i),$$

with the associated errors where C_i are the number of source counts in the i-th PSPC PI energy channel. The scatter plot of HR_2 vs. HR_1 is shown in the left panel of Fig. 7; the solid symbols indicate the three sources for which we have been able to perform spectral fits. In the right panel we show the model-predicted behaviour of the hardness ratios as a function of source temperature and interstellar absorption. It is worth to note that

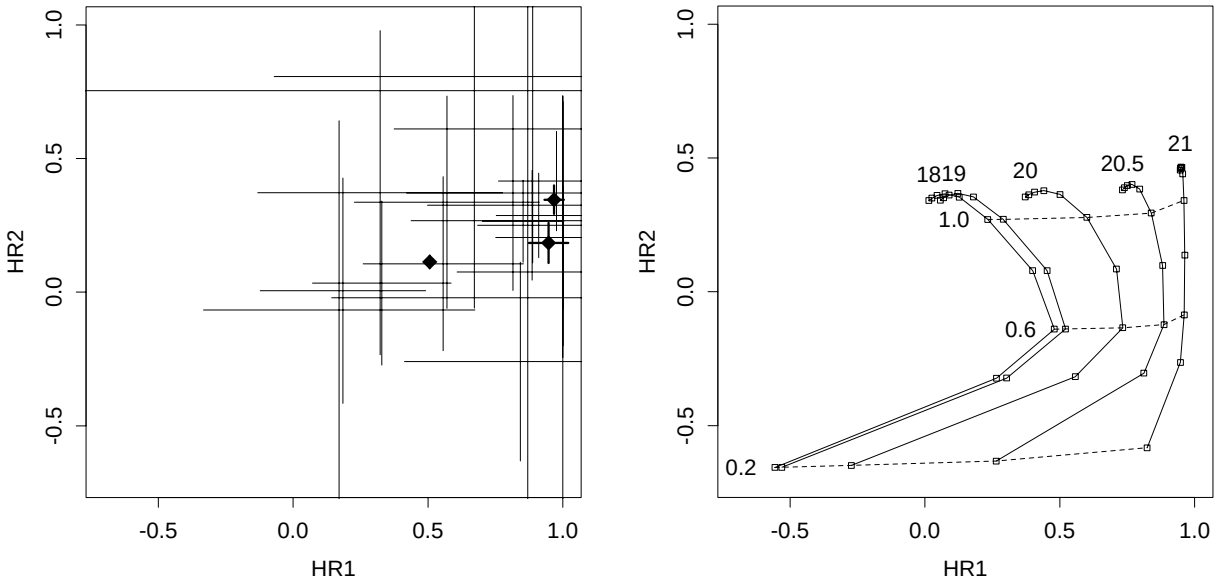

Fig. 7. [left panel] Scatter plot of the source hardness ratios. The solid symbols indicate the three sources for which we have performed spectral fits. [right panel] The predicted behaviour of the HR_1 vs. HR_2 for a single temperature optically thin plasma whose emission is described with the Raymond-Smith emission model and for various values of interstellar absorption. The hardness ratio have been computed for temperature in the range 0.2–2.0 keV with step of 0.2 keV, and for Log N_H in the range 18–21 cm^{-2}. Numbers above curves indicate the value of Log N_H, the number on the left the temperature (in keV) of the plasma.

Table 6. Summary of spectral fit results

Source ID	Obs ID	KT_{low} [keV]	KT_{high} [keV]	EM_{low}/EM_{high}	Log N_H [cm^{-2}]	χ^2/ν	f_X 10^{-12} erg/cm^2/s [0.2 - 2.0 keV]
USco-010	Summed	...	1.01± 0.23	...	$19.78\pm^{0.05}_{0.06}$	148.5/26	4.61
		0.15±0.02	0.99±0.04	0.64	$20.43\pm^{0.11}_{0.14}$	27.48/24	5.58
USco-014	Summed	...	1.38± 0.11	...	$20.94\pm^{0.13}_{0.18}$	29.20/26	1.27
USco-041	Summed	...	$1.02\pm^{0.17}_{0.32}$	...	$20.70\pm^{0.22}_{0.26}$	16.15/26	1.38

the many sources that occupy the same region of the two sources for which the single temperature fits results in a plasma with temperature around 1 keV and Log $N_H \sim$ 20.7-21.0, must have similar values of temperature and absorption, i.e. they must be quite hard (for a coronal source) and have value of absorption compatible with being at the distance of Upper Sco-Cen. On the other hand, the nature of the sources with (HR_1, HR_2) near (0.3,0.1) is less clear, since this region can be populated either by soft sources subject only to a small amount of absorption, or by sources with a more complex spectrum (with at least two dominant temperatures clearly distinguishable. e.g. USco-010) whose hardness ratio would be the emission measure weighted mean of those corresponding to the two (or more) dominating temperatures (cf. Collura et al., 1995).

5. Catalog identifications

All the sources in the final list have been tentatively identified through positional matching with a list of catalogued objects in the surveyed region. This list has been extracted from a catalog containing more than 1.5 10^6 objects that has been purposely assembled for an ongoing project of a systematic re-analysis of ROSAT pointed data (Mackie et al. 1995, 1996) and that includes positions and other relevant data taken from more than 43 optical, radio, infrared and X-ray catalogs among others. The list of X-ray sources has been also matched with the objects listed in the GSC V1.1 (Lasker et al., 1990) and we have taken advantage of the list of identifications of WVMBM for part of the IPC sources. All the resulting catalog identifications are listed in Table 7.

For 25 sources this match results in at least one catalogued object falling in the X-ray error circle offering a possible counterparts. However, since in many cases the catalogued objects are quite faint (and the GSC V1.1 is far from being complete at these magnitudes), other objects of similar magnitude can fall in the error circle, as it is illustrated by the finding charts in the appendix.

For the remaining X-ray sources we have not been able to find any catalogued objects falling in the error circle. A quick look to the finding charts of these sources, that are marked with an '*', reveals that in many cases a plausible counterpart is present anyway.

Table 7. Catalog identifications for the X-ray sources in the surveyed region

X-ray ID	Name(1)	m_v	Offset ["]	SC ID's(2)	m_{GSC} range	Offset ["]
USco-004	...	...	...	2	14.0-15.4	85.0-106.3
USco-005	...	...	...	1	14.9	20.9
USco-006	HD 142184	5.42	10.4	1	5.40	10.8
USco-008	...	...	...	2	13.8-14.3	42.6-44.7
USco-010	W005	8.96		1	9.3	2.1
" "	SAO 183920	8.80	0.4	0	...	...
USco-014	W008	14.2	14.0	1	8.2	5.83
" "	SAO 183927	8.5	6.1			
USco-017	...	...	...	1	13.30	52.7
USco-018	...	...	...	1	8.2	6.7
USco-024	...	...	...	2	14.6-14.9	51-52
USco-027	W013	13.01	2.6	1	14.4	2.9
USco-031	W014	15.45	6.0	0	...	...
USco-032	...	...	...	1	15.1	3.4
USco-033	...	...	...	1	15.0	8.3
USco-034	W015	12.78	4.6	1	13.9	3.4
USco-035	W016	13.72		3	14.6-14.9	23.2-66.8
USco-037	W017	13.63	1.3	1	14.4	6.1
USco-039	...	...	...	1	13.5	3.0
USco-041	SAO 183978	9.50	18.9	1	11.10	19.1
USco-043	HBC 608	10.50	7.2	1	10.5	4.9
USco-044	W019	13.25		0	...	...
USco-045	HD 143275	2.32		0	...	...
USco-046	W020	13.74		0	...	...
USco-047	W021	11.45		0	...	...
USco-049	W022	14.09		0	...	...
USco-050	W023	11.32		0	...	...

(1) - The name starting with W indicate the counterpart listed by WVMBM; HBC indicates stars listed in the Herbig & Robbin-Bell catalog (1988)

(2) - We list the number of stars listed in the GSC V1.1 falling in the X-ray error circle. The last two columns summarize the ranges of magnitude (in the natural J band system of the GSC plate) and offset from the X-ray position for the possible GSC counterparts.

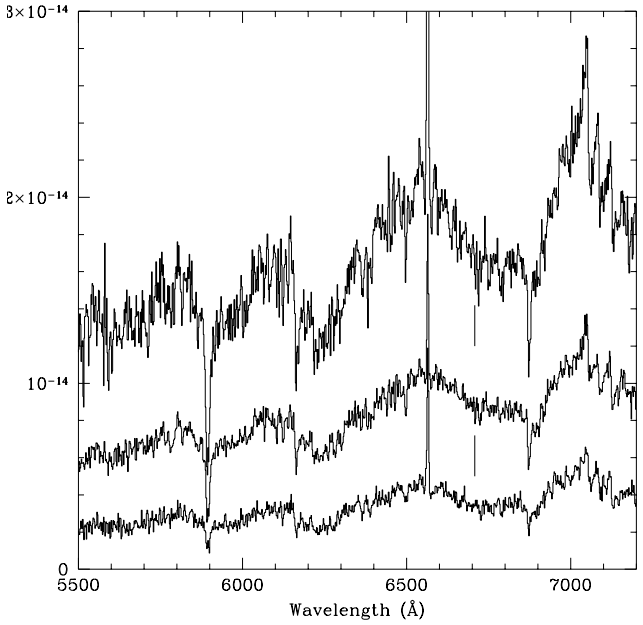

Fig. 8. The optical spectra of three of the faint X-ray sources in the Sco-Cen region. The vertical axis is calibrated in absolute flux, and is in erg cm^{-2} s^{-1} Å^{-1}. The sources, falling in the IPC field I5936, are USco-013 (bottom), USco-025 (middle) and USco-037 (top). The Li I line (indicated by a vertical line in the plots) is clearly visible in the two brighter sources even at the low resolution of the spectra, implying a very high lithium abundance. Given the M spectral type of these stars this is indicative of their PMS status. The H_α emission confirms the high activity level of these stars.

6. Optical observations of faint X-ray sources

As noted previously, in addition to the X-ray sources reported by WVMBM, the final analysis of Einstein IPC observations allows to detect five lower statistics X-ray sources, four of which have been confirmed by the new ROSAT observations. In an effort to assess whether the existing census of PMS sources was reasonably complete we observed the optical counterparts to these five lower statistics IPC sources in the field I5936 (which overlaps our ROSAT HRI observation). We performed low resolution spectroscopic observations of the potential optical counterparts of these faint X-ray sources using the Boller and Chivens spectrograph at the ESO 1.5 m telescope, at a resolution of ≈ 1.9 Å per pixel. Each spectrum covers all the optical region, from ≈ 3800 Å to ≈ 8000 Å. The observations were performed on January 30, 1994, and were reduced in the usual way.

The strong indication from these preliminary optical observations (a larger dedicated optical program being already scheduled for an observing season in June 1997) is that a significant fraction (two out of four) of these sources turns out to be low-mass M-type PMS stars. The spectra of two faint X-ray sources in the Sco-Cen region, which are not in WVMBM (although falling in the region of the sky surveyed by them) and yet are clearly low-mass PMS stars, are shown in Fig. 8. The source USco-025 (middle spectrum in Fig. 8) is confirmed as an X-ray source by the ROSAT HRI observation presented here, the source USco-013 (lower spectrum), falling outside our ROSAT HRI observation, is confirmed by the PSPC observation. The upper spectrum in Fig. 8 belongs to the counterpart of source USco-037 of our list. This source has been studied previously by WVMBM and has identified with the same PMS star (star 017 in their list) whose spectrum we report for comparison.

The three objects reported here show clearly the characteristics of low-mass PMS stars. They are of spectral type M, with clearly visible TiO bands, have strong Hα emission, and the lithium 6707.8 Å absorption line is clearly visible (in the top two spectra) even at such low spectral resolution, implying a large lithium abundance which, at the low masses of these stars, is only compatible with a PMS status[4]. The signal to noise ratio

[4] Favata et al., (1997) have shown that while low-resolution spectra can hardly be adopted to recognize PMS stars of G and K spectral type

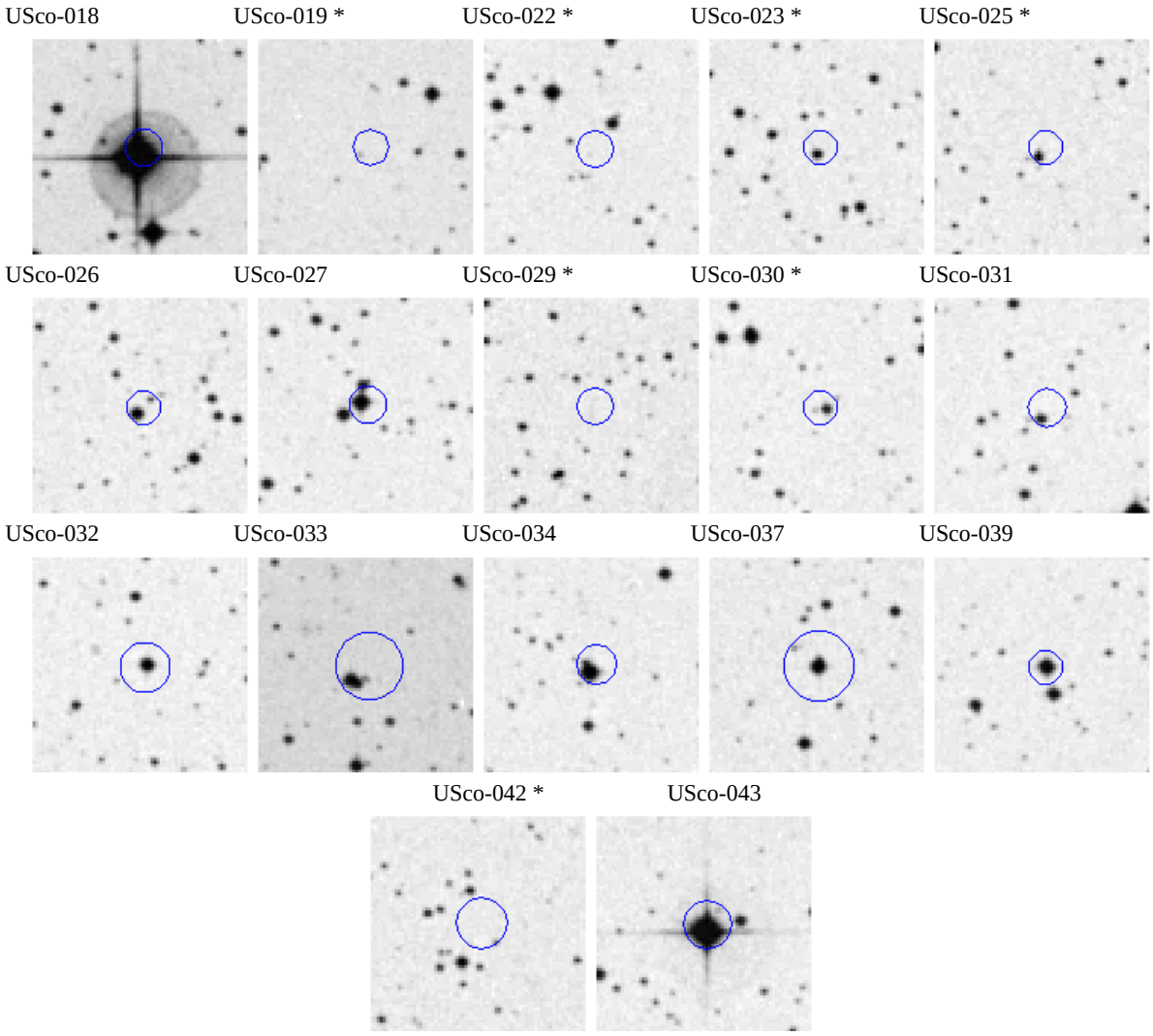

Fig. A1. Finding charts for the 17 HRI sources detected in the Upper Sco-Cen Association region, extracted from the STScI DSS, with overlaid the 90% confidence positional error circle. Each chart is 2' on a side. An asterisk on the upper right corner indicates those sources for which no catalog identification has been found.

of the lower spectrum is too low to allow for the lithium line to be detected.

The two other sources (USco-009 and USco-018) have multiple optical counterparts (some of which are too faint to be observed in the little time we had available). The brighter optical counterparts appear to be normal main sequence stars. However, it is possible that the fainter, unobserved potential counterparts are also PMS sources. Further observations in the next season would allow us to enlarge the size of the identified sample and to derive firmer conclusions on the fraction of M type PMS stars in the Upper Sco-Cen association.

searching for the lithium 6707.8 Å absorption line, this is feasible for M type PMS stars

7. Conclusions

The analysis of X-ray data of the Upper Sco Cen region shows that (at least) a fraction of the X-ray sources have spectral and variability characteristics similar to that of typical PMS stars, and this suggestion is further reinforced by the analysis of the limited optical data we have available. The inspection of the finding charts (in the Appendix) and of catalogs identifications shows that most of the likely counterparts are stars with magnitude typically in the range m_V=14-17, and given the X-ray flux of sources these translate in objects with log f_X/f_V typically in the -2.5 – 0.5 range, i.e. in the range where we expect that a number of PMS stars falls (cf. Fig. 2 of Sterzick et al. (1995)). While any definitive statement must wait for the results of the already planned optical follow-up observational campaign that will allow to identify through 1 Å resolution spectroscopy the spectral types, lithium abundance and radial velocities of the counter-

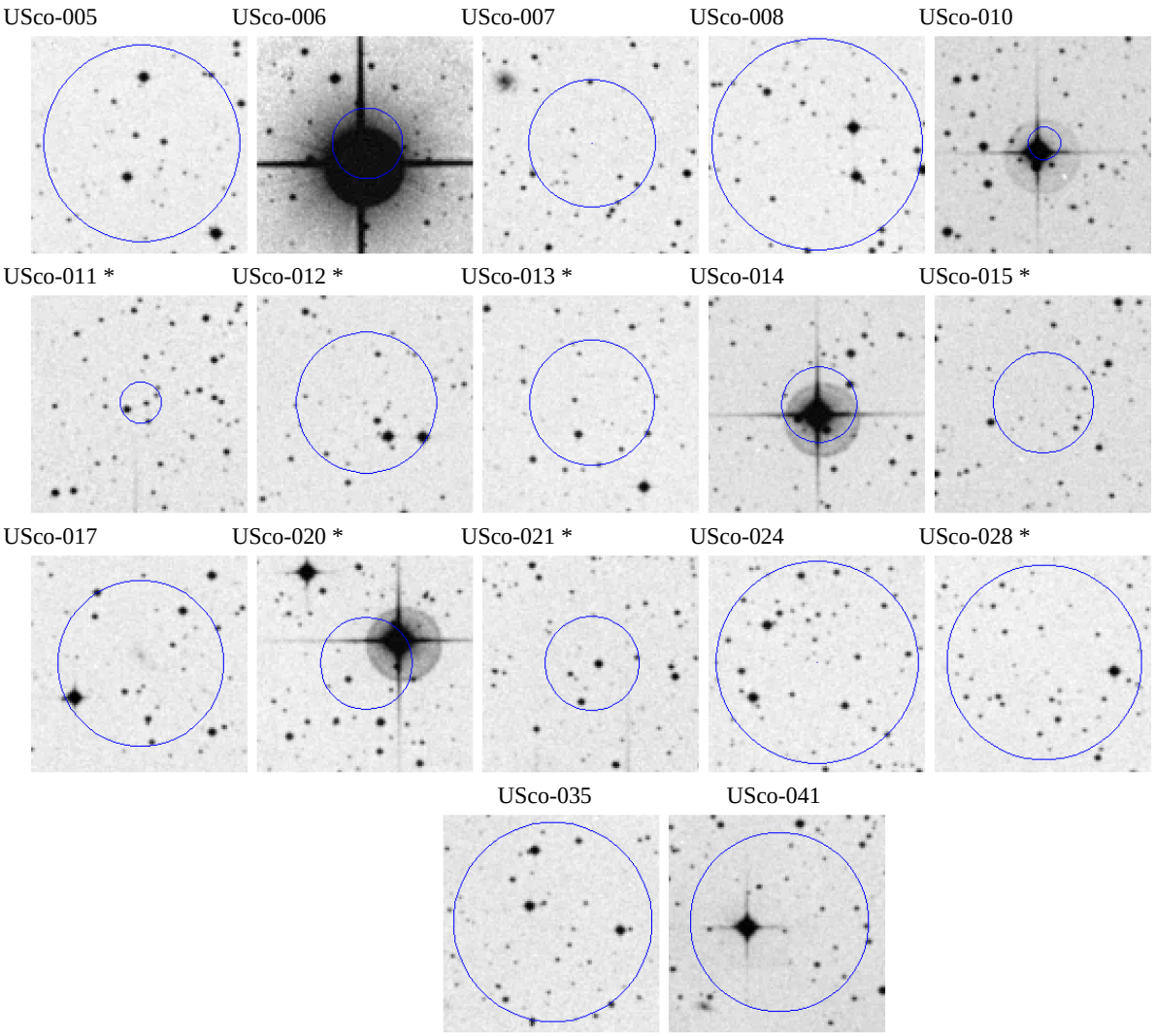

Fig. A2. Finding charts for the 17 PSPC sources detected in the Upper Sco-Cen Association region extracted from the ST ScI DSS, with overlaid the 90% confidence positional error circle. Each chart is 3' on a side. Only those sources with an error circle smaller than 90" in radius are shown. An asterisk on the upper right corner indicates those sources for which no catalog identification has been found.

parts, we have shown that the Einstein observations (as well the shallow RASS data) are far from having given a complete characterization of the X-ray population of the Upper Sco-Cen SFR. The new optical data will allow to determine whether the new X-ray sources (a) are low mass stars, or (b) X-ray fainter members with the same mass and age as the population studied by WVMBM, or (c) X-ray fainter members with the same masses as the population studied by WVMBM but significantly older. Under hypothesis "a" we would be able to constrain a truly *initial* mass function at the lower masses ($M < M_{\odot}$), under hypothesis "b" WVMBM's IMF need to be revised as the new data would allow us to determine a more reliable IMF, while under hypothesis "c" the current view of the whole star-formation history of the Sco-Cen SFR would need to be revisited. Either of the three possibilities would thus lead to a significant improvement in the understanding of low mass star formation by studying stars at very young ages (≈ 1 Myr) in one of the few SFR in which this is not hampered by dust and residual gas.

Acknowledgements. F. D., G. M. and S. S. acknowledge support from the ASI (Italian Space Agency), MURST and GNA-CNR. We acknowledge the usage of the photographic data obtained using The UK Schmidt Telescope and the STScI digitization and compression.

Appendix A: findings charts and "identification" with Palomar survey

In order to ease the identification work we have produced for most of the X-ray sources in our list finding charts based on the STScI Digitized Sky Survey CD-ROMs. These findings charts are shown in Fig. A1 for all HRI sources, while in Fig. A2 we show the finding charts for the 17 PSPC sources in our list whose 90% confidence positional error circles have a radius smaller than 90". For the other 7 PSPC sources without an HRI

counterpart and falling in the outer part of the field of view the radius of the error circle is larger and likely prevents any sensible optical identification program.

References

Barbera M., Collura A., Dara A., et al., 1997, Experimental Astronomy 7, 51

Blaauw A., 1991, in The Physics of Star Formation and early Stellar Evolution, C. J. Lada and N. D. Kylafis (eds.,) Kluwer, Dordrecht, 125

Branduardi-Raymont G., Mason K. O., Warwick R. S. et al., 1994, MNRAS 270, 947

Briel U. G., Aschenbach B., Hasinger G., et al., 1996, The ROSAT Users' Handbook

Carkner L., Feigelson E. D., Koyama K., Montmerle T., Reid I. N., 1996, ApJ 464, 286

Collura A., Micela G., Sciortino S., Harnden F.R. Jr., Rosner R., 1995, ApJ 446, 108.

Damiani F., Maggio A., Micela G., Sciortino S., 1996a, in Röntgenstrahlung from the Universe, H. U. Zimmermann, J. E. Trümper, H. Yorke (eds), MPE Report 263, p. 679

Damiani F., Maggio A., Micela G., Sciortino S., 1996b, in Astronomical Data Analysis Software and Systems V, G.H. Jacoby, J. Barnes (eds), ASP Conf. Ser. 101, p. 143

Damiani F., Maggio A., Micela G., Sciortino S., 1997a, ApJ 483, 350

Damiani F., Maggio A., Micela G., Sciortino S., 1997b, ApJ 483, 370

David L. P., Harnden F. R. Jr., Kearns K. E., Zombeck M. V., 1993, The Rosat High Resolution Imager (HRI).

de Geus E. J., 1992, A&A 262, 258

de Geus E. J., de Zeeuw P. T., Lub J., 1989, A&A 216, 44

Favata F., Micela G., Sciortino S., G.S. Vaiana, 1992, A&A 256, 86

Favata F., Micela G., Sciortino S., 1997, A&A 326, 647

Feigelson E., D., Casanova S., Montmerle T., Guibert J., 1993, ApJ 416, 623

Gagné M., Caillault J-P., Stauffer J. R., 1995a, ApJ 450, 217

Gagné M., Caillault J-P., Stauffer J. R., 1995b, ApJ 445, 280

Guillolt P., Haywood M., Motch C., Robin A. C., 1996, A&A 316, 89

Grosso N., Montmerle T., Feigelson E. D. et al., 1997, Nat 387, 56

Harnden F. R. Jr., Fabricant D. G., Harris D. E., Schwartz J., 1984, SAO Special Report, n. 393

Harnden F. R. Jr., Sciortino S., Micela G., et al., 1990, In Elvis, M., editor, *Imaging X-ray Astronomy*, Cambridge University Press, p. 313

Harris D. E, Forman W., Gioia I. M., et al., 1990, The Einstein Observatory Catalog of IPC X-Ray Sources, NASA TM 108401

Hasinger G., Boese G., Predehl P., et al., 1993a, MPE/OGIP Calibration Memo CAL/ROS/93-015.

Hasinger G., Burg R., Giacconi R. et al., 1993b, A&A 275, 1

Herbig G. H., Robbin-Bell K. 1988, Third Catalog of Emission-Line Stars of the Orion Population, Lick Obs. Bull. n. 1111

Lasker B. M., Sturch C. R., Mclean B. J., et al., 1990, AJ 99, 2019

Mackie G., Fabbiano G., Bocchino F., et al., 1995, in Röntgenstrahlung from the Universe, H. U. Zimmermann, J. E. Trümper, H. Yorke (eds), MPE Report 263, p. 385

Mackie G., Fabbiano G., Barbera M., et al., 1996, in Proceedings of the meeting "Astronomical Data Analysis Software and Systems V", G.H. Jacoby and J. Barnes (eds.), p. 179

Micela G., 1991, PhD. Thesis, University of Palermo

Micela, G., Sciortino, S., Vaiana, G.S. et al., 1988, ApJ 325, 798

Micela G., Sciortino S., Favata F., 1993, ApJ 618, 412

Micela G., Sciortino S., Kashyap V., Harnden F.R.,Jr., Rosner R., 1995, ApJS 102, 75

Micela G., Pye J., Sciortino S., 1997, A&A 320, 865

Montmerle T., Koch-Miramond L., Falgarone E., Grindlay J. E., 1983, ApJ 269, 182

Pfefferman E., Briel U. G., Hippman H., et al., 1986, Proc. SPIE 733, 519

Preibisch T., 1997a, A&A 324, 690

Preibisch T., 1997b, A&A 320, 525

Preibisch T., Zinnecker H., Schmitt J.H.M.M., 1993, A&A 279, 33

Preibisch T., Neuhäuser R., Alcalà J. M., 1995, A&A 304, 13

Schmitt J. H. M. M., Kahabka, P., Stauffer, J., Peiters, A., 1993, A&A 277, 114

Sciortino S., Micela G., 1992, ApJ 388, 595

Sciortino S., Harnden F. R. Jr., Maggio A., et al., 1988, in Astronomy from Large Databases, F. Murtagh, & A. Heck (eds), p. 483

Sciortino S., Micela G., Kashyap V., Harnden F.R.,Jr., Rosner R., 1994, in ASP Conf. Proc. 64, Cool Stars, Stellar System, and the Sun, ed. J.-P. Caillault (San Francisco: ASP), 140

Sciortino S., F. Favata, Micela G., 1995, A&A 296, 370

Snowden S. L., McCammon D., Burrows D. N., Mendenhall J. A., 1994, ApJ 424, 714

Stark, A.A., et al., 1992, ApJS 79, 77

Sterzik M. F., Alcalá J. M., Neuhäuser R., Schmitt J.H.M.M., 1995, A&A 297, 418.

Vaiana G. S. 1983, in Solar and stellar magnetic fields: Origins and coronal effects, J.O. Stenflo (ed.), Reidel, p. 165

Voges W., Aschenbach, B., Boller Th., et al., 1997, A&A, in press

Walter F. M., Vrba F. J., Mathieu R. D., Brown A., Myers P. C., 1994, AJ 107, 692 (WVMBM)

Zombeck M.V., Barbera M., Collura A., Murray S.S., 1997, ApJL, in press.

This article was processed by the author using Springer-Verlag LaTeX A&A style file *L-AA* version 3.